

Solution Structure of Domain 1.1 of the  $\sigma^A$  Factor from *Bacillus subtilis* is Preformed for Binding to the RNA Polymerase Core

Milan Zachrdla<sup>12</sup>, Petr Padrta<sup>12</sup>, Alžbeta Rabatinová<sup>3</sup>, Hana Šanderová<sup>3</sup>, Ivan Barvík<sup>4</sup>, Libor Krásný<sup>3</sup>, Lukáš Židek<sup>12</sup>

From the <sup>1</sup>CEITEC - Central European Institute of Technology, Masaryk University, Kamenice 5, CZ-62500 Brno, Czech Republic and the <sup>2</sup>NCBR, Faculty of Science, Masaryk University, Kamenice 5, CZ-62500 Brno, Czech Republic and the <sup>3</sup>Laboratory of Microbial Genetics and Gene Expression, Institute of Microbiology, The Czech Academy of Sciences, CZ-14220 Prague 4, Czech Republic and the <sup>4</sup>Division of Biomolecular Physics, Institute of Physics, Faculty of Mathematics and Physics, Charles University, Ke Karlovu 5, CZ-12116 Prague 2, Czech Republic

Running title: *Structure of Domain  $\sigma 1.1$  from *B. subtilis**

To whom correspondence should be addressed: Libor Krásný, Laboratory of Microbial Genetics and Gene Expression, Institute of Microbiology, The Czech Academy of Sciences, CZ-14220 Prague 4, Czech Republic, Telephone: +420 241 063 208, E-mail: krasny@biomed.cas.cz and Lukáš Židek, CEITEC - Central European Institute of Technology, Masaryk University, Kamenice 5, CZ-62500 Brno, Czech Republic and NCBR, Faculty of Science, Masaryk University, Kamenice 5, CZ-62500 Brno, Czech Republic, Telephone: +420 549 49 8393, E-mail: lzidek@chemi.muni.cz.

**Keywords:** protein structure, nuclear magnetic resonance (NMR), RNA polymerase, *Bacillus*, transcription initiation factor, molecular modeling

## ABSTRACT

Bacterial RNA polymerase (RNAP) requires  $\sigma$  factors to recognize promoter sequences. Domain 1.1 of primary  $\sigma$  factors ( $\sigma 1.1$ ) prevents their binding to promoter DNA in the absence of RNAP, and when in complex with RNAP, it occupies RNAP's DNA-binding channel. Currently, two 3D structures of  $\sigma 1.1$  are available: from *Escherichia coli* in complex with RNAP and from *Thermotoga maritima* solved free in solution. However, these two structures significantly differ, and it is unclear whether this difference is due to an altered conformation upon RNAP binding or to differences in intrinsic properties between the proteins from these two distantly related species. Here, we report the solution structure of  $\sigma 1.1$  from the Gram-positive bacterium *Bacillus subtilis*. We found that *B. subtilis*  $\sigma 1.1$  is highly compact because of additional stabilization not present in  $\sigma 1.1$  from the other two species and that it is more similar to *E. coli*  $\sigma 1.1$ . Moreover, modeling studies suggested that *B. subtilis*  $\sigma 1.1$  requires minimal conformational changes for accom-

modating RNAP in the DNA channel, whereas *T. maritima*  $\sigma 1.1$  must be rearranged to fit therein. Thus, the mesophilic species *B. subtilis* and *E. coli* share the same  $\sigma 1.1$  fold, whereas the fold of  $\sigma 1.1$  from the thermophile *T. maritima* is distinctly different. Finally, we describe an intriguing similarity between  $\sigma 1.1$  and  $\delta$ , an RNAP-associated protein in *B. subtilis*, bearing implications for the so far unknown binding site of  $\delta$  on RNAP. In conclusion, our results shed light on the conformational changes of  $\sigma 1.1$  required for its accommodation within bacterial RNAP.

Transcription of DNA into RNA is an essential cellular process. It is mediated by DNA dependent RNA polymerase (RNAP). RNAP is a multisubunit enzyme, and in bacteria the RNAP core is composed of five subunits ( $2\alpha$ ,  $\beta$ ,  $\beta'$ ,  $\omega$ ). Gram positive Firmicutes contain two additional subunits,  $\delta$  and  $\epsilon$  (1). A number of functions have been ascribed to  $\delta$ , including affecting affinity of RNAP for

DNA (2) and for initiating nucleoside triphosphates (3) or functioning as a transcription factor (4). The absence of  $\delta$  decreases competitive fitness and virulence (3, 5). The effects of  $\delta$  are augmented by HelD, a helicase-like protein associating with RNAP (6). The function of  $\epsilon$  is less clear (6, 7). The RNAP core is capable of transcription elongation but it is not able to bind to promoter DNA, where transcription begins. For RNAP to bind to promoter DNA, the presence of a  $\sigma$  factor is necessary. Upon a  $\sigma$  factor binding to the RNAP core, the resulting RNAP holoenzyme is capable of recognizing promoter sequences and subsequently initiating transcription (8). Preventing the binding of  $\sigma$  factors to the RNAP core is also used as a strategy for development of novel antibacterial compounds (9).

Different bacterial species contain different numbers of different  $\sigma$  factors, ranging from one per species to more than 100 (10). According to their structure,  $\sigma$  factors are divided into two principally distinct groups,  $\sigma^{70}$  and  $\sigma^{54}$  families. Factors from the  $\sigma^{54}$  family have no sequence similarity with  $\sigma^{70}$  factors and they require the binding of ATP-dependent activators (11). Factors from the  $\sigma^{70}$  family are present in all bacterial species and no ATP-dependent activators are needed. The  $\sigma^{70}$  family is further subdivided into four groups (1–4), based on domain composition. Group 1 contains vegetative  $\sigma$  factors ( $\sigma^{70}$  in *Escherichia coli*,  $\sigma^A$  in *Bacillus subtilis*), essential for transcription of housekeeping genes. Groups 2–4 contain structurally-related alternative  $\sigma$  factors responsible for transcription of genes whose expression is important during various environmental stresses (10, 11).

The vegetative  $\sigma$  factors (group 1) contain four domains: domain 1.1, domain 2 (regions 1.2–2.4), domain 3 (regions 3.0–3.2) and domain 4 (regions 4.1–4.2). Regions 2.4 (domain 2) and 4.2 (domain 4) recognize the –10 and –35 promoter consensus hexamer sequences, respectively, that are critical for the initial RNAP-DNA binding (closed complex) and subsequent formation of the transcription bubble, the so called open complex. Region 1.2 (domain 2) interacts with the DNA region between the transcription start site (+1) and the –10 hexamer, and affects the stability of the open complex. Domain 3 binds to the –10 extended motif (TGx). This motif precedes the –10 hexamer and it is not present

in all promoters. When it is present, however, it increases the promoter's affinity for RNAP and boosts transcription (10).

When  $\sigma^A$  binds to RNAP that is not in complex with DNA,  $\sigma$ 1.1 occupies the DNA binding channel (12, 13). Further,  $\sigma$ 1.1 plays a specific role in autoregulation of the  $\sigma$  factor. It inhibits the binding of the  $\sigma$  factor to promoter DNA sequence alone. Trans binding experiments with the *E. coli*  $\sigma$ 1.1 region and truncated  $\sigma^{70}$  variants suggested that  $\sigma$ 1.1 binds to domain 4 (region 4.2) in free state (14). Furthermore, examination of possible interdomain interactions of *Thermotoga maritima*  $\sigma$  factor as studied by an interdomain crosslinking approach suggested that  $\sigma$ 1.1 is in a close proximity to domains 2 and 4 (15). Molecular details of these interactions, however, are still elusive.

Currently, two structures of  $\sigma$ 1.1 are available, one from *T. maritima* solved by NMR (15), and the other from *E. coli* solved by crystallography in complex with RNAP (12). Despite sequence similarities in  $\sigma$ 1.1 in these two organisms, their 3D structures differ. In both organisms, this domain consists of three helices (HI–HIII) connected by two loops. However, while in *T. maritima* HII and HIII are roughly anti-parallel to one another and pack perpendicularly against HI, in *E. coli* the three helices show anti-parallel packing, leading to a distinctly different morphology.

Here, to provide a basis for better understanding of the structural diversity among  $\sigma$  domains 1.1 from different species that could have implications for their binding to RNAP, we solved the solution structure of  $\sigma^A$  domain 1.1 from the model soil-dwelling gram positive bacterium *B. subtilis*.

## RESULTS

**$\sigma$ 1.1 structure determination** — We decided to solve the structure of  $\sigma$ 1.1 by NMR due to its small size (9.4 kDa) and the benefit of getting additional information on flexibility of the protein. Despite the high occurrence of Glu and Gln residues in the  $\sigma$ 1.1 sequence, an almost complete backbone and side-chain assignment was obtained. As expected, overlapped peaks from the His-Tag and missing peaks from the N-terminal residue were not assigned; otherwise only two backbone and four side-chain chemical shifts remained unassigned. Spectra measured

on a diluted sample confirmed the monomeric state of the sample. NOE assignment yielded 1886 unambiguous  $^1\text{H}$ - $^1\text{H}$  distances, including 486 long-range NOEs. Additional restraints, 21  $^3J_{\text{HNHA}}$  and 86 RDC values, were used for the residues that were predicted to form  $\alpha$ -helices. The calculated structure is in agreement with the secondary structure prediction from chemical shifts. Statistics of the structure calculation is presented in Table 1.

**Structure of  $\sigma 1.1$** —The first 71 amino acids of *B. subtilis*  $\sigma 1.1$  form three helices (Helix I: F12 to R26, Helix II: Y31 to F41, Helix III: S45 to E57) that are connected by two short loops (Fig. 1). The HI-HII loop is formed by amino acids G27–T30 and the HII-HIII loop is formed by amino acids E42–E44. The N-terminus (amino acids A1–T11) and C-terminus (amino acids Q58–D71) are mainly unstructured. An important exception is a small portion of the C-terminus (amino acids  $^{61}\text{ELI}^{63}$ ), which together with the HI-HII loop (residues  $^{28}\text{VLT}^{30}$ ) forms a  $\beta$ -sheet motif that is stabilized via hydrogen bonding between the respective parts of the  $\sigma 1.1$  main chain. The total charge of the 71 amino-acid *B. subtilis*  $\sigma 1.1$  is  $-15$ , i.e.,  $-21 \times (\text{E or D}) + 6 \times (\text{K or R})$ . The frequency of negatively charged amino acids is increasing from the N-terminus to the C-terminus. While Helix I is still slightly positively charged ( $+1$ ), the remaining structural motifs display progressively increasing negative charge: the N-terminus ( $-1$ ), Helix II ( $-2$ ), HII-HIII ( $-2$ ), Helix III ( $-5$ ) and the C-terminus ( $-6$ ). It is therefore clear that the *B. subtilis*  $\sigma 1.1$  can mimic a portion of downstream duplex DNA that is also strongly negatively charged due to the presence of phosphate groups in the phosphodiester bonds between nucleotides.

**$^{15}\text{N}$  relaxation**—NMR relaxation was used to probe the dynamics of the  $\sigma 1.1$  domain. A set of  $^{15}\text{N}$  relaxation rates, including  $R_1$  and  $R_2$  autorelaxation rates, steady state  $\{^1\text{H}\}$ - $^{15}\text{N}$  heteronuclear Overhauser enhancement (ssNOE), and longitudinal and transverse cross-correlated relaxation rates, was measured (16). The software relax was used to analyze the relaxation data in the model-free manner (17–20). The analysis showed that the molecule tumbles as a prolate spheroid, with the global correlation time ( $1/6D_{\text{iso}}$ ) of 6.13 ns at 25 °C and with  $D_{\parallel}/D_{\perp}$  of 2.23. Internal dynamics of individual

residues was characterized by the order parameter  $S^2$  and the effective correlation time  $\tau_e$  (Fig. 2). The decrease of the order parameter  $S^2$  values, indicating more flexible regions, was observed in the loop between  $\alpha$ -helices II and III, as well as in the  $\beta$ -sheets. In many cases, introduction of a second mode of internal motion, described by an additional order parameter and correlation time, resulted in a statistically significant improvement of the fit. The correlation time of the second mode was well defined in the terminal regions ( $\tau_s \approx 1$  ns), but determined with a large uncertainty in the well-ordered regions (Fig. 2B). Also, the analysis provided significant exchange contribution ( $R_{\text{ex}}$ ) for many residues (Fig. 2C), indicating a presence of a slow conformational exchange in Helix I (especially in its terminal regions) and in the proximal regions (C-terminal portion of the Helix II,  $\beta$ -sheet II and its vicinity). In summary, the model-free analysis revealed that the internal motions of  $\sigma 1.1$  are more complex than typical for well-structured proteins. Therefore, molecular motions on a slow timescale (ms- $\mu$ s) were studied in more detail, using the  $^{15}\text{N}$  relaxation dispersion Carr-Purcell-Meiboom-Gill sequence (CPMG) experiment analyzed in the software relax (20). The analysis confirmed the presence of a conformational exchange, sufficiently well described by a two-state model with a relatively uniform exchange rate of approximately 3,500 Hz and with the minor state being populated by 1.5 % (Fig. 3). The  $^{15}\text{N}$  chemical shift differences between both states varied from 2 ppm to 6 ppm, with the most significant changes at the end of Helix I, in the Helix II and  $\beta$ -sheet II.

**Position of  $\sigma 1.1$  within the DNA binding channel of RNAP**—In RNAP which is not bound to DNA,  $\sigma 1.1$  is positioned inside the DNA binding channel (12, 13). To gain insights into the position of *B. subtilis*  $\sigma 1.1$  within *B. subtilis* RNAP, we carried out structural alignments using the software package Molsoft (www.molsoft.com). As a template we used the crystal structure of *E. coli* RNAP (PDB ID 4LK1; (12)). Our NMR structure of *B. subtilis*  $\sigma 1.1$  and a previously published homology model of *B. subtilis* RNAP core (21) were structurally aligned with the template.

In this model, *B. subtilis*  $\sigma 1.1$  occupies the downstream duplex DNA binding channel with its center of gravity at approximately  $+8$  ( $+1$  is the tran-

scription start site), where it must be displaced by the DNA upon formation of the open promoter complex. It is wedged in the RNAP channel, interacting with the  $\beta$  subunit (i.e. amino acids D151, R183, R188, R241 and R498), and with structural elements of the  $\beta'$  subunit, namely the  $\beta'$  clamp (I110, R123), the rudder around residue 301, and two amino acid residues of the  $\beta'$ -pincer (K1125, R1144). Many salt bridges stabilizing *B. subtilis*  $\sigma 1.1$  in the downstream DNA binding channel of the RNAP core can be predicted based on our model, involving Helix I, II, and especially Helix III (core RNAP /  $\sigma 1.1$ ): D151 / R26, R183 / E36, R188 / E42, R241 / E42, R498 / E65, I110 / F54, R123 / E50, R300 – R301 – R303 / E44 E50 D46, K1125 and R1144 / E57 (see Fig. 4A).

While the position of the structured part of *B. subtilis*  $\sigma 1.1$  within the DNA channel can be well predicted, the position of the unstructured C-terminus of the *B. subtilis*  $\sigma 1.1$  (the linker to  $\sigma 1.2$ ) can be only roughly approximated. Nevertheless, it is apparent that the C-terminus of  $\sigma 1.1$  would interact with mobile and functionally important parts of the RNAP core, namely with the Bridge Helix (responsible for the DNA:RNA translocation), and with the Trigger Loop (opening or closing access of NTP into the active site of RNAP through the secondary channel). The C-terminus of the *B. subtilis*  $\sigma 1.1$  contains many negatively charged amino acids (for example E67, E68, E70, D71, E73) that could create additional salt bridges with a number of positively charged amino acid residues in the Bridge Helix (R784, K785, K793, R802, R803) and in the Trigger Loop (R937, R955, R963) (see Fig. 4A).

## DISCUSSION

We have determined the solution structure of  $\sigma 1.1$ , the N-terminal domain of the primary  $\sigma$  factor,  $\sigma^A$ , from *B. subtilis*. For a long time, the structure of this domain had not been available due to its flexibility until it was solved by NMR for *T. maritima* (15), and, several years later, also by crystallography for *E. coli* (12). In the crystal structure,  $\sigma 1.1$  is a part of  $\sigma^{70}$ , in a context of a complex with RNAP. The two known structures (*E. coli* and *T. maritima*) differ significantly. In the following text, we provide detailed comparisons of *B. subtilis*  $\sigma 1.1$  with these two structures. The comparisons shed light

on interactions and conformational changes of  $\sigma 1.1$  required for  $\sigma 1.1$  accommodation within RNAP.

*$\sigma 1.1$  sequence comparisons*—The  $\sigma 1.1$  domains from *B. subtilis*, *E. coli* and *T. maritima* displayed a modest degree of sequence similarity except for the non-conserved N-terminus (residues ~1–30) of *T. maritima* (*B. subtilis* and *E. coli* lack this fragment). Pairwise alignments of respective sequences from *B. subtilis*, *E. coli*, and *T. maritima* revealed a sequence identity of about 25 %. Multiple alignment of these sequences then yielded a sequence identity of only around 10 %. Nevertheless, it should be noted that in the case of E/D amino acid residues, which we believe are critical for the binding of  $\sigma 1.1$  to the RNAP core, there are numerous point substitutions which do not change charge (either E to D or D to E – seven occasions for *B. subtilis* vs. *E. coli*, see Fig. 1). Moreover, these amino acids are often shifted just by one position in the  $\sigma 1.1$  sequences (five occasions for *T. maritima* vs. *B. subtilis* and *E. coli*, see Fig. 1). These evolutionary differences mean that the sequence similarity is significantly greater than the sequence identity. Taking into account that their interaction counterparts in salt bridges are positively charged amino acids with long flexible side chains (either Lys or Arg), such subtle variations are unlikely to affect the  $\sigma 1.1$  function(s). The highest sequence conservation is around the HI–HII loop region (L19, G23, K24, G27, T30, Y31).

*$\sigma 1.1$  structure comparisons*—The 3D solution structure of *B. subtilis*  $\sigma 1.1$  resembles the crystal structure of *E. coli*  $\sigma 1.1$ , that was obtained in the context of RNAP (Fig. 5). Despite the similarities, Helix I in *B. subtilis*  $\sigma 1.1$  is slightly longer than Helix I in *E. coli*  $\sigma 1.1$  (12). Furthermore, several interactions that contribute to anchoring Helix I to the rest of the structure of *B. subtilis*  $\sigma 1.1$  are missing in *E. coli*  $\sigma 1.1$ . These interactions are mediated by F12, whose bulky side chain is nestled between side chains of M38, F41, and I43 of the HII–HIII loop (Fig. 1).

The *B. subtilis* and *E. coli* structures then markedly differ from that one of *T. maritima* where HI packs perpendicularly to HII and HIII. This contrasts with the all-anti-parallel packing of helices in *B. subtilis* and *E. coli*  $\sigma 1.1$  (Fig. 5). It should be noted that HI from *T. maritima*  $\sigma 1.1$  is by far



the longest one, and it is also preceded by the non-conserved and unstructured N-terminus.

**$\sigma 1.1$  interactions with RNAP**—Predicted salt bridges between *B. subtilis*  $\sigma 1.1$  and the DNA channel have corresponding analogous interactions in the structure of *E. coli* RNAP (PDB ID 4LK1; (12) compare Fig. 4A and Fig. 4B).

The compact structure of *B. subtilis*  $\sigma 1.1$  is undoubtedly important for its optimal interactions with the RNAP core in the downstream DNA binding channel (especially salt bridges formed by E57, E65, R26 and E42) (Fig. 4A). The compact structure likely compensates for the absence of some additional parts of RNAP (including those of  $\sigma 1.1$ ) that are found uniquely in either *E. coli* or *T. maritima* and that participate in positioning of  $\sigma 1.1$  in the DNA channel by reducing the breathing movements of RNAP cleft arms. The “extra” part of *E. coli* RNAP consists of a large insertion (i.e. amino acids G938 to T1131, see PDB ID 4YLN; (22)) in the Trigger Loop that regulates access of NTPs into the RNAP active site via the secondary channel. The “extra” part of *T. maritima* RNAP is the relatively long N-terminus of its  $\sigma 1.1$ , which was unstructured in the solution structure of isolated  $\sigma 1.1$  (15).

Remarkably, HI of *T. maritima*  $\sigma 1.1$  apparently does not fit into the downstream DNA channel of RNAP (Fig. S1) whereas HI of *B. subtilis*  $\sigma 1.1$  fits this space smoothly (Fig. 4C, Fig. S1). It indicates that HI of *T. maritima*  $\sigma 1.1$  likely undergoes a conformational change to be accommodated into the RNAP core.

Interestingly, the structure of *T. maritima*  $\sigma 1.1$  is very similar to the structured N-terminal part of the  $\delta$  subunit of *B. subtilis* RNAP, consisting of four alpha-helices (Helices Ia, Ib, II, and III, formed by residues Q8–K12, L16–H27, F33–L44, G52–N63, respectively). In fact, helices Ia+Ib, II and III of  $\delta$  correspond to HI, HII and HIII of *T. maritima*  $\sigma 1.1$ , respectively (Fig. 5 and Fig. S2). In addition,  $\delta$  contains a short anti-parallel  $\beta$ -sheet composed of three short  $\beta$ -strands (residues V31–P32, F68–A70 and T75–L78) at the top of a “twisted tripod” formed by Helices Ib, II, and III) (23–25) (Fig. 5). This motif structurally overlaps with the short two-strand  $\beta$ -sheet found in our NMR structure of *B. subtilis*  $\sigma 1.1$ . Future experiments will have to reveal whether the apparent structure sim-

ilarity between  $\sigma 1.1$  and  $\delta$  may provide clues for identifications of the so far unknown binding site of  $\delta$  on RNAP.

In conclusion, the determined solution structure of *B. subtilis*  $\sigma 1.1$  showed for the first time a preformed 3D conformation that requires minimal, if any, conformational changes to be accommodated within the DNA binding channel. Moreover, the NMR relaxation revealed that the determined structure of  $\sigma 1.1$  is in a slow exchange with a minor state, differing mostly in the Helix HI and its proximity. One can speculate that the minor state may resemble the solved structure of  $\sigma 1.1$  from *T. maritima*. However, further experiments are needed to test this hypothesis.

## EXPERIMENTAL PROCEDURES

**Sample preparation**— $\sigma 1.1$  was prepared using a standard protocol including cloning, expression, and purification methods to produce a  $^{13}\text{C}$ ,  $^{15}\text{N}$ -uniformly labeled sample in a sufficient concentration. The truncated gene of the  $\sigma^A$  coding only its  $\sigma 1.1$  part (amino acids 1–71) was cloned into a pET28b vector between NcoI and XhoI sites. The additional six histidine residues at the C-terminus served as the His-tag facilitating the protein purification process, and the two residues preceding the His-tag (LE) were inserted because of the restriction enzyme (XhoI) used for cloning.

**NMR measurements**—All NMR experiments were performed at 25 °C using 0.8 mM  $^{13}\text{C}$ ,  $^{15}\text{N}$ -labeled sample or 0.6 mM  $^{15}\text{N}$ -labeled sample. Temperature was calibrated according to the chemical shift differences of pure methanol peaks.

Resonance assignment was done using experiments acquired on 700 MHz Bruker Avance III spectrometer equipped with the TXO cryogenic probehead with z-axis gradients and 850 MHz Bruker Avance III spectrometer equipped with the TCI cryogenic probehead with z-axis gradients. Standard set of 3D triple-resonance experiments HNCA, HN(CO)CA, HNCO, HNCACB, and CBCA(CO)NH (26) was used for backbone assignment. Multiple experiments for side-chain assignment, HCCH-TOCSY, TOCSY-HSQC,  $^{13}\text{C}$ -edited aromatic NOESY-HSQC, H(CC)(CO)NH, and (H)CC(CO)NH (26) were employed to overcome chemical shift degeneracies due to a high

occurrence of Glu and Gln residues in the sequence. Assignment of all obtained chemical shifts was deposited in the BioMagResBank ([http://www.bmrb.wisc.edu](http://www.bmrb.wisc.edu;);(27)) under the accession code 34089.

Protein structure calculation was based on  $^1\text{H}$ - $^1\text{H}$  distance restraints obtained from  $^{15}\text{N}$ -edited NOESY-HSQC and  $^{13}\text{C}$ -edited NOESY-HSQC (for both aromatic and aliphatic spectral regions) experiments (26). In addition, three-bond scalar couplings, obtained from HNHA experiment (28), were used to determine  $\phi$  torsion angles of the protein backbone.  $^1D(\text{HN}^{\text{H}})$ ,  $^1D(\text{C}^{\alpha}\text{C}')$ ,  $^1D(\text{NC}')$ , and  $^2D(\text{H}^{\text{N}}\text{C})$  residual dipolar couplings (RDCs) were obtained from  $^1\text{H}$ ,  $^{15}\text{N}$ -IPAP, HN[C]-S3E, and  $^{13}\text{C}$ -detected (H)CACO-IPAP experiments run on the isotropic sample and on a sample partially oriented in 5 % polyacrylamide gel. Program S3EPY (29) was used to evaluate RDCs obtained from the measured spectra. The (non-uniform) RDC errors were estimated from 1D lineshape using Cramer-Rao lower bound theory (30). Spectra were processed using the program NMRPipe 8.1 (31) and analyzed using the program Sparky 3.115 (T. D. Goddard and D. G. Kneller, University of California, San Francisco, USA). Secondary structure prediction utilizing  $^{13}\text{C}^{\alpha}$ ,  $^{13}\text{C}^{\beta}$ ,  $^{13}\text{C}'$ ,  $^1\text{H}$ , and  $^{15}\text{N}$  chemical shifts was done using program ssp 1.0 (32). Automated assignment of NOESY spectra was performed using CANDID (33), an algorithm included in the program CYANA (34). CNS 1.2 (35) was used for refinement of structures in water using RECOORD scripts modified for our needs (36). Module TENSO (37) was used to include RDCs into structure calculation. Both  $^3J_{\text{HNHA}}$  and RDCs were used only for residues in  $\alpha$ -helices. 300 initial structures were calculated and 150 structures with the lowest energy were further refined using an explicit water model. The final ensemble of 20 structures with the lowest energy was validated using program CING (38, 39) and deposited in the Protein Data Bank ([www.rcsb.org](http://www.rcsb.org);(40)) under the PDB ID 5MWW.

NMR relaxation experiments were performed at a 600 MHz Bruker Avance III spectrometer equipped with the QCI cryogenic probehead with z-axis gradients, at a 850 MHz Bruker Avance III spectrometer equipped with the TCI cryogenic probehead with z-axis gradients, and at a 950 MHz

Bruker Avance III spectrometer equipped with the TCI cryogenic probehead with z-axis gradients. The overall number of 2048 complex points was acquired in the acquisition dimension and 320 complex points were acquired in the indirect dimension for auto-relaxation rates  $R_1$ ,  $R_2$  and steady-state  $^{15}\text{N}$ - $^1\text{H}$  nuclear Overhauser effect. Standard experiments (16) were used for the measurement of  $R_1$  (relaxation delays 11.1, 55.5, 133.2, 233.1, 377.4, 555, 888\*, 1942.5 ms) and  $R_2$  with the delay between the 180 pulses in the CPMG train equal to 0.83 ms (relaxation delays 0, 14.4, 28.8, 43.2\*, 57.6, 72, 86.4 ms). Asterisks denote spectra recorded twice in order to estimate experimental error. The ssNOE values were measured under a steady-state condition, achieved by a 5 ms  $^1\text{H}$  irradiation with 226 repeats of 200  $\mu\text{s}$   $180^\circ$   $^1\text{H}$  pulses (41), separated by 22.22 ms delays, and with a 30 s interscan relaxation delay. Reference spectra and the spectra measured under steady-state conditions were measured in an interleaved manner.

Transverse cross-correlated relaxation rates  $\Gamma_x$  (relaxation delays 30, 50, and 70 ms) and longitudinal cross-correlated relaxation rates  $\Gamma_z$  (relaxation delays 100, 175, and 250 ms) were obtained using experiments based on symmetrical reconversion (42, 43). Programs relax (44–47) and Octave (48) were used to obtain relaxation rates by fitting peak intensities to a monoexponential decay.

Consistency of the relaxation data was tested as proposed by Morin and Gagné (49). The field independent  $J(0)$  values obtained from the auto-correlated and cross-correlated relaxation rates by the spectral density mapping show that the data were not biased by imperfect temperature calibration during the measurements at different magnetic fields. The model-free analysis (17–19) of auto-relaxation rates from 600 MHz, 850 MHz, and 950 MHz was performed using the d'Auvergne protocol in the software relax. The prolate diffusion model was selected based on the lowest value of the Akaike's Information Criterion (50). The selected model was then used to estimate errors of calculated parameters by performing 500 Monte Carlo simulations. Relaxation rates and model-free order parameters were deposited in the BioMagResBank under accession number 27011. Relaxation dispersion CPMG experiments with CPMG frequency ranging from 111 to 2,000 Hz (51) were acquired and an-

alyzed using the relaxation dispersion auto-analysis in the software relax (20) to study the slow exchange.

*In silico modelling* — Structural alignments were produced using the ICM Molsoft software

package (www.molsoft.com). Amino acids sequences were aligned using the Clustal Omega web server (<http://www.ebi.ac.uk/Tools/msa/clustalo/>).

**Acknowledgments:** This work was supported by Czech Science Foundation, grant number GA 13-16842S and by the Ministry of Education, Youth and Sports of the Czech Republic (MEYS CR) under the National Sustainability Programme II, project CEITEC 2020 (LQ1601). CIISB research infrastructure project LM2015043 funded by MEYS CR is gratefully acknowledged for a partial financial support of the measurements at the Josef Dadok National NMR Centre, CEITEC - Masaryk University.

**Conflict of interest:** The authors declare that they have no conflicts of interest with the contents of this article.

**Author contributions:** MZ, LK, and LZ conceived and designed the research, AR, HS, and LK prepared the samples, MZ, PP, and LZ acquired and analyzed the NMR data and solved the structure, IB did the in-silico modeling, MZ, IB, LK, and LZ wrote the manuscript. All authors reviewed and contributed to the manuscript.

## REFERENCES

1. Weiss, A. and Shaw, L. N. (2015) Small things considered: the small accessory subunits of RNA polymerase in Gram-positive bacteria, *FEMS microbiology reviews* **39**(4), 541–554. 10.1093/femsre/fuv005
2. de Saro, F. J. L., Woody, A.-Y. M., and Helmann, J. D. (1995) Structural Analysis of the *Bacillus subtilis*  $\delta$  Factor: A Protein Polyanion which Displaces RNA from RNA Polymerase, *J. Mol. Biol.* **252**(2), 189 – 202. 10.1006/jmbi.1995.0487
3. Rabatinová, A., Šanderová, H., Jirát Matějčková, J., Korelusová, J., Sojka, L., Barvík, I., Papoušková, V., Sklenář, V., Židek, L., and Krásný, L. (2013) The  $\delta$  Subunit of RNA Polymerase Is Required for Rapid Changes in Gene Expression and Competitive Fitness of the Cell, *J. Bacteriol.* **195**. 10.1128/JB.00188-13
4. Prajapati, R. K., Sengupta, S., Rudra, P., and Mukhopadhyay, J. (2015) *Bacillus subtilis*  $\delta$  functions as a transcriptional regulator by facilitating the open complex formation, *J. Biol. Chem.* 10.1074/jbc.M115.686170
5. Weiss, A., Ibarra, J. A., Paoletti, J., Carroll, R. K., and Shaw, L. N. (2014) The  $\delta$  Subunit of RNA Polymerase Guides Promoter Selectivity and Virulence in *Staphylococcus aureus*, *Infect. Immun.* **82**(4), 1424–1435. 10.1128/IAI.01508-14
6. Wiedermannová, J., Sudzinová, P., Kovaľ, T., Rabatinová, A., Šanderová, H., Ramaniuk, O., Rittich, Š., Dohnálek, J., Fu, Z., Halada, P., Lewis, P., and Krásný, L. (2014) Characterization of heldD, an interacting partner of RNA polymerase from *Bacillus subtilis*, *Nucleic Acids Res.* **42**(8), 5151. 10.1093/nar/gku113
7. Keller, A. N., Yang, X., Wiedermannová, J., Delumeau, O., Krásný, L., and Lewis, P. J. (2014)  $\epsilon$ , a New Subunit of RNA Polymerase Found in Gram-Positive Bacteria, *J. Bacteriol.* **196**(20), 3622–3632. 10.1128/JB.02020-14
8. Murakami, K. S. and Darst, S. A. (2003) Bacterial {RNA} polymerases: the whole story, *Curr. Opin. Struct. Biol.* **13**(1), 31 – 39. 10.1016/S0959-440X(02)00005-2
9. Ma, C., Yang, X., Kandemir, H., Mielczarek, M., Johnston, E. B., Griffith, R., Kumar, N., and Lewis, P. J. (2013) Inhibitors of Bacterial Transcription Initiation Complex Formation, *ACS Chem. Biol.* **8**(9), 1972–1980. 10.1021/cb400231p
10. Paget, M. S. (2015) Bacterial Sigma Factors and Anti-Sigma Factors: Structure, Function and Distribution, *Biomol.* **5**(3), 1245. 10.3390/biom5031245
11. Österberg, S., del Peso-Santos, T., and Shingler, V. (2011) Regulation of Alternative Sigma Factor Use, *Annu. Rev. Microbiol.* **65**, 37–55. 10.1146/annurev.micro.112408.134219
12. Bae, B., Davis, E., Brown, D., Campbell, E., Wigneshweraraj, S., and S.A., D. (2013) Phage T7 Gp2 inhibition of *Escherichia coli* RNA polymerase involves misappropriation of  $\sigma^{70}$  domain 1.1, *Chem. Biol.* **110**, 19,772–19,777. 10.1073/pnas.1314576110
13. Murakami, K. (2013) X-ray Crystal Structure of *Escherichia coli* RNA Polymerase  $\sigma^{70}$  Holoenzyme, *The J. Biol. Chem.* **288**, 9126–9134. 10.1074/jbc.M112.430900
14. Dombroski, A., Walter, W., and Gross, C. (1993) Amino-terminal amino acids modulate  $\sigma$ -factor DNA-binding activity, *Genes Dev.* **7**(12 A), 2446–2455. 10.1101/gad.7.12a.2446
15. Schwartz, E., Shekhtman, A., Dutta, K., Pratt, M., Cowburn, D., Darst, S., and Muir, T. (2008) A Full-Length Group 1 Bacterial Sigma Factor Adopts a Compact Structure Incompatible with DNA Binding, *Chem. Biol.* **15**(10), 1091–1103. 10.1016/j.chembiol.2008.09.008
16. Korzhnev, D., Billeter, M., Arseniev, A., and Orekhov, V. (2001) {NMR} studies of brownian tumbling and internal motions in proteins, *Prog. Nucl. Magn. Reson. Spectrosc.* **38**(3), 197 – 266. 10.1016/S0079-6565(00)00028-5
17. Lipari, G. and Szabo, A. (1982) Model-Free Approach to the Interpretation of Nuclear Magnetic Resonance Relaxation in Macromolecules. 1. Theory and Range of Validity, *J. Am. Chem. Soc.*



- 104**(17), 4546–4559. 10.1021/ja00381a009
18. Lipari, G. and Szabo, A. (1982) Model-Free Approach to the Interpretation of Nuclear Magnetic Resonance Relaxation in Macromolecules. 2. Analysis of Experimental Results, *J. Am. Chem. Soc.* **104**(17), 4559–4570. 10.1021/ja00381a010
  19. Clore, G. M., Szabo, A., Bax, A., Kay, L. E., Driscoll, P. C., and Gronenborn, A. M. (1990) Deviations from the Simple Two-Parameter Model-Free Approach to the Interpretation of Nitrogen-15 Nuclear Magnetic Relaxation of Proteins, *J. Am. Chem. Soc.* **112**(12), 4989–4991. 10.1021/ja00168a070
  20. Morin, S., Linnet, T. E., Lescanne, M., Schanda, P., Thompson, G. S., Tollinger, M., Teilum, K., Gagné, S., Marion, D., Griesinger, C., Blackledge, M., and d’Auvergne, E. J. (2014) relax: the analysis of biomolecular kinetics and thermodynamics using NMR relaxation dispersion data, *Bioinforma.* **30**(15), 2219. 10.1093/bioinformatics/btu166
  21. MacDougall, I. J., Lewis, P. J., and Griffith, R. (2005) Homology modelling of RNA polymerase and associated transcription factors from *Bacillus subtilis*, *J. Mol. Graph. Model.* **23**(4), 297 – 303. 10.1016/j.jmgm.2004.10.001
  22. Zuo, Y. and Steitz, T. (2015) Crystal Structures of the *E.coli* Transcription Initiation Complexes with a Complete Bubble, *Mol. Cell* **58**(3), 534 – 540. 10.1016/j.molcel.2015.03.010
  23. Demo, G., Papoušková, V., Komárek, J., Kadeřávek, P., Otrusínová, O., Srb, P., Rabatinová, A., Krásný, L., Žídek, L., Sklenář, V., and Wimmerová, M. (2014) X-ray vs. NMR structure of N-terminal domain of  $\delta$ -subunit of RNA polymerase, *J. Struct. Biol.* **187**. 10.1016/j.jsb.2014.06.001
  24. Papoušková, V., Kadeřávek, P., Otrusínová, O., Rabatinová, A., Šanderová, H., Nováček, J., Krásný, L., Sklenář, V., and Žídek, L. (2013) Structural Study of the Partially Disordered Full-Length  $\delta$  Subunit of RNA Polymerase from *Bacillus subtilis*, *ChemBioChem* **14**. 10.1002/cbic.201300226
  25. Motáčková, V., Šanderová, H., Žídek, L., Nováček, J., Padrta, P., Švenková, A., Korelusová, J., Jonák, J., Krásný, L., and Sklenář, V. (2010) Solution structure of the N-terminal domain of *Bacillus subtilis*  $\delta$  subunit of RNA polymerase and its classification based on structural homologs, *Proteins* **78**, 1807–1810. 10.1002/prot.22708
  26. Sattler, M., Schleucher, J., and Griesinger, C. (1999) Heteronuclear multidimensional NMR experiments for the structure determination of proteins in solution employing pulsed field gradients, *Prog. Nucl. Magn. Reson. Spectrosc.* **34**(2), 93–158. 10.1016/s0079-6565(98)00025-9
  27. Ulrich, E. L., Akutsu, H., Doreleijers, J. F., Harano, Y., Ioannidis, Y. E., Lin, J., Livny, M., Mading, S., Maziuk, D., Miller, Z., Nakatani, E., Schulte, C. F., Tolmie, D. E., Kent Wenger, R., Yao, H., and Markley, J. L. (2008) BioMagResBank, *Nucleic Acids Res.* **36**(suppl 1), D402–D408. 10.1093/nar/gkm957
  28. Vuister, G. W. and Bax, A. (1993) Quantitative  $J$  Correlation: a New Approach for Measuring Homonuclear Three-Bond  $J(\text{H}^{\text{N}}\text{H}^{\alpha})$  Coupling Constants in  $^{15}\text{N}$ -Enriched Proteins, *J. Am. Chem. Soc.* **115**(17), 7772–7777. 10.1021/ja00070a024
  29. Novák, P., Žídek, L., Motáčková, V., Padrta, P., Švenková, A., Nuzillard, J.-M., Krásný, L., and Sklenář, V. (2010) S3EPY: a Sparky extension for determination of small scalar couplings from spin-state-selective excitation NMR experiments, *J. Biomol. NMR* **46**(2), 191–197. 10.1007/s10858-009-9392-1
  30. Hagen, N., Kupinski, M., and Dereniak, E. L. (2007) Gaussian profile estimation in one dimension, *Appl. Opt.* **46**(22), 5374–5383. 10.1364/AO.46.005374
  31. Delaglio, F., Grzesiek, S., Vuister, G. W., Zhu, G., Pfeifer, J., and Bax, A. (1995) NMRPipe: A multidimensional spectral processing system based on UNIX pipes, *J. Biomol. NMR* **6**(3), 277–293. 10.1007/BF00197809
  32. Marsh, J., Singh, V., Jia, Z., and Forman-Kay, J. (2006) Sensitivity of secondary structure propensities to sequence differences between  $\alpha$ - and  $\gamma$ -synuclein: Implications for fibrillation, *Protein*

- Sci.* **15**(12), 2795–804. 10.1110/ps.062465306
33. Herrmann, T., Güntert, P., and Wüthrich, K. (2002) Protein NMR structure determination with automated NOE assignment using the new software CANDID and the torsion angle dynamics algorithm DYANA, *J. Mol. Biol.* **319**(1), 209 – 227. 10.1016/S0022-2836(02)00241-3
  34. Güntert, P. and Buchner, L. (2015) Combined automated NOE assignment and structure calculation with CYANA, *J. Biomol. NMR* **62**(4), 453–471. 10.1007/s10858-015-9924-9
  35. Brünger, A. T., Adams, P. D., Clore, G. M., DeLano, W. L., Gros, P., Grosse Kunstleve, R. W., Jiang, J. S., Kuszewski, J., Nilges, M., Pannu, N. S., Read, R. J., Rice, L. M., Simonson, T., and Warren, G. L. (1998) *Crystallography & NMR System: A New Software Suite for Macromolecular Structure Determination*, *Acta Crystallogr. Sect. D* **54**(5), 905–921. 10.1107/s0907444998003254
  36. Jansen, S., Chmelfik, J., Židek, L., Padrt, P., Novák, P., Zdráhal, Z., Picimbon, J., François, Löfstedt, C., and Sklenář, V. (2007) Structure of *Bombyx mori* Chemosensory Protein 1 in Solution, *Arch. Insect Biochem. Physiol.* **66**. 10.1002/arch.20205
  37. Sass, H.-J., Musco, G., Stahl, S. J., Wingfield, P. T., and Grzesiek, S. (2001) An easy way to include weak alignment constraints into NMR structure calculations, *J. Biomol. NMR* **21**(3), 275–280. 10.1023/A:1012998006281
  38. Doreleijers, J. F., Vranken, W. F., Schulte, C., Markley, J. L., Ulrich, E. L., Vriend, G., and Vuister, G. W. (2012) NRG-CING: integrated validation reports of remediated experimental biomolecular NMR data and coordinates in wwPDB, *Nucleic Acids Res.* **40**(D1), D519–D524. 10.1093/nar/gkr1134
  39. Doreleijers, J. F., Sousa da Silva, A. W., Krieger, E., Nabuurs, S. B., Spronk, C. A. E. M., Stevens, T. J., Vranken, W. F., Vriend, G., and Vuister, G. W. (2012) CING: an integrated residue-based structure validation program suite, *J. Biomol. NMR* **54**(3), 267–283. 10.1007/s10858-012-9669-7
  40. Berman, H. M., Westbrook, J., Feng, Z., Gilliland, G., Bhat, T. N., Weissig, H., Shindyalov, I. N., and Bourne, P. E. (2000) The Protein Data Bank, *Nucleic Acids Res.* **28**(1), 235–242. 10.1093/nar/28.1.235
  41. Ferrage, F., Cowburn, D., and Ghose, R. (2009) Accurate Sampling of High-Frequency Motions in Proteins by Steady-State  $^{15}\text{N}$ - $^1\text{H}$  Nuclear Overhauser Effect Measurements in the Presence of Cross-Correlated Relaxation, *J. Am. Chem. Soc.* **131**(17), 6048–6049. 10.1021/ja809526q
  42. Pelulessy, P., Espallargas, G. M., and Bodenhausen, G. (2003) Symmetrical reconversion: measuring cross-correlation rates with enhanced accuracy, *J. Magn. Reson.* **161**(2), 258 – 264. 10.1016/S1090-7807(02)00190-8
  43. Pelulessy, P., Ferrage, F., and Bodenhausen, G. (2007) Accurate measurement of longitudinal cross-relaxation rates in nuclear magnetic resonance, *The J. Chem. Phys.* **126**(13), 134508. 10.1063/1.2715583
  44. d’Auvergne, E. J. and Gooley, P. R. (2006) Model-free model elimination: A new step in the model-free dynamic analysis of NMR relaxation data, *J. Biomol. NMR* **35**(2), 117. 10.1007/s10858-006-9007-z
  45. d’Auvergne, E. J. and Gooley, P. R. (2007) Set theory formulation of the model-free problem and the diffusion seeded model-free paradigm, *Mol. BioSyst.* **3**, 483–494. 10.1039/B702202F
  46. d’Auvergne, E. J. and Gooley, P. R. (2007) Optimisation of NMR dynamic models I. Minimisation algorithms and their performance within the model-free and Brownian rotational diffusion spaces, *J. Biomol. NMR* **40**(2), 107. 10.1007/s10858-007-9214-2
  47. d’Auvergne, E. J. and Gooley, P. R. (2008) Optimisation of NMR dynamic models II. A new methodology for the dual optimisation of the model-free parameters and the Brownian rotational diffusion tensor, *J. Biomol. NMR* **40**(2), 121–133. 10.1007/s10858-007-9213-3
  48. Eaton, J. W., Bateman, D., and Hauberg, S. (2008) *GNU Octave Manual Version 3*, Network Theory Ltd.

49. Morin, S. and M. Gagné, S. (2009) Simple tests for the validation of multiple field spin relaxation data, *J. Biomol. NMR* **45**(4), 361. 10.1007/s10858-009-9381-4
50. d'Auvergne, E. J. and Gooley, P. R. (2003) The use of model selection in the model-free analysis of protein dynamics, *J. Biomol. NMR* **25**(1), 25–39. 10.1023/A:1021902006114
51. Long, D., Liu, M., and Yang, D. (2008) Accurately Probing Slow Motions on Millisecond Timescales with a Robust NMR Relaxation Experiment, *J. Am. Chem. Soc.* **130**(8), 2432–2433. 10.1021/ja710477h

## TABLES

**Table 1:** Structure calculation statistics.

Parameters	Number/Value
NMR assignment (%)	
Backbone nuclei*	> 99 %
Side-chain nuclei*	> 99 %
Restraints	
Total NOE	1886
short-range, $ i - j  \leq 1$	925
medium-range, $1 <  i - j  < 5$	475
long-range, $ i - j  \geq 5$	486
$^3J_{\text{HNHA}}$	21
RDC	86
Average violations**	
NOE > 0.5 Å	0.0
$^3J_{\text{HNHA}} > 3\sigma^{***}$	0.0
RDC > $3\sigma^{***}$	0.0
RMSD to the mean structure**	
backbone atoms	(0.38 ± 0.10) Å
heavy atoms	(1.01 ± 0.14) Å
Ramachandran diagram statistics**	
Most favourite region	96.3 %
Additional favored region	3.6 %
Generously allowed region	0.1 %
Disallowed region	0.0 %

\*Assignment statistics was obtained without including His-tag. \*\*Structured part only (residues 10–63) was analyzed for the final ensemble of 20 structures. \*\*\*Violations of scalar and residual dipolar couplings were evaluated using standard deviation of the experimental data.

## FIGURES

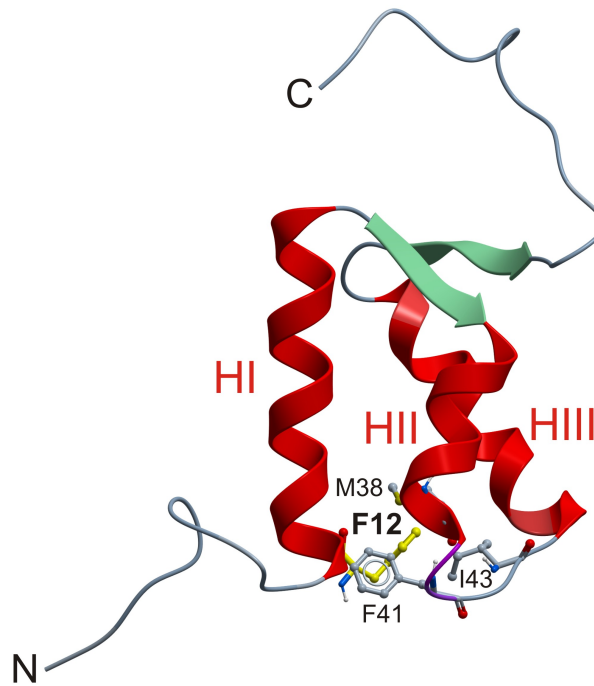
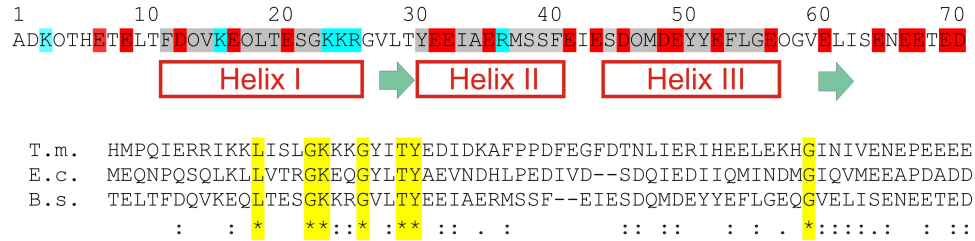


**Figure 1:**  $\sigma 1.1$  of *B. subtilis*. (A) Amino acid sequence of *B. subtilis*  $\sigma 1.1$  with helices indicated below the sequence. Negatively charged residues are shown in red, positively charged residues in blue. An alignment of amino acid sequences from *T. maritima*, *E. coli*, and *B. subtilis* is shown below. Asterisks (\*) indicate fully conserved amino acid residues, colons (:) indicate conservation of amino acid residues with strongly similar properties, and dots (.) indicate conservation of amino acid residues with weakly similar properties. (B) Solution structure of  $\sigma 1.1$  of *B. subtilis*. Helices HI–HIII, N-/C-termini and selected amino acid residues are indicated.



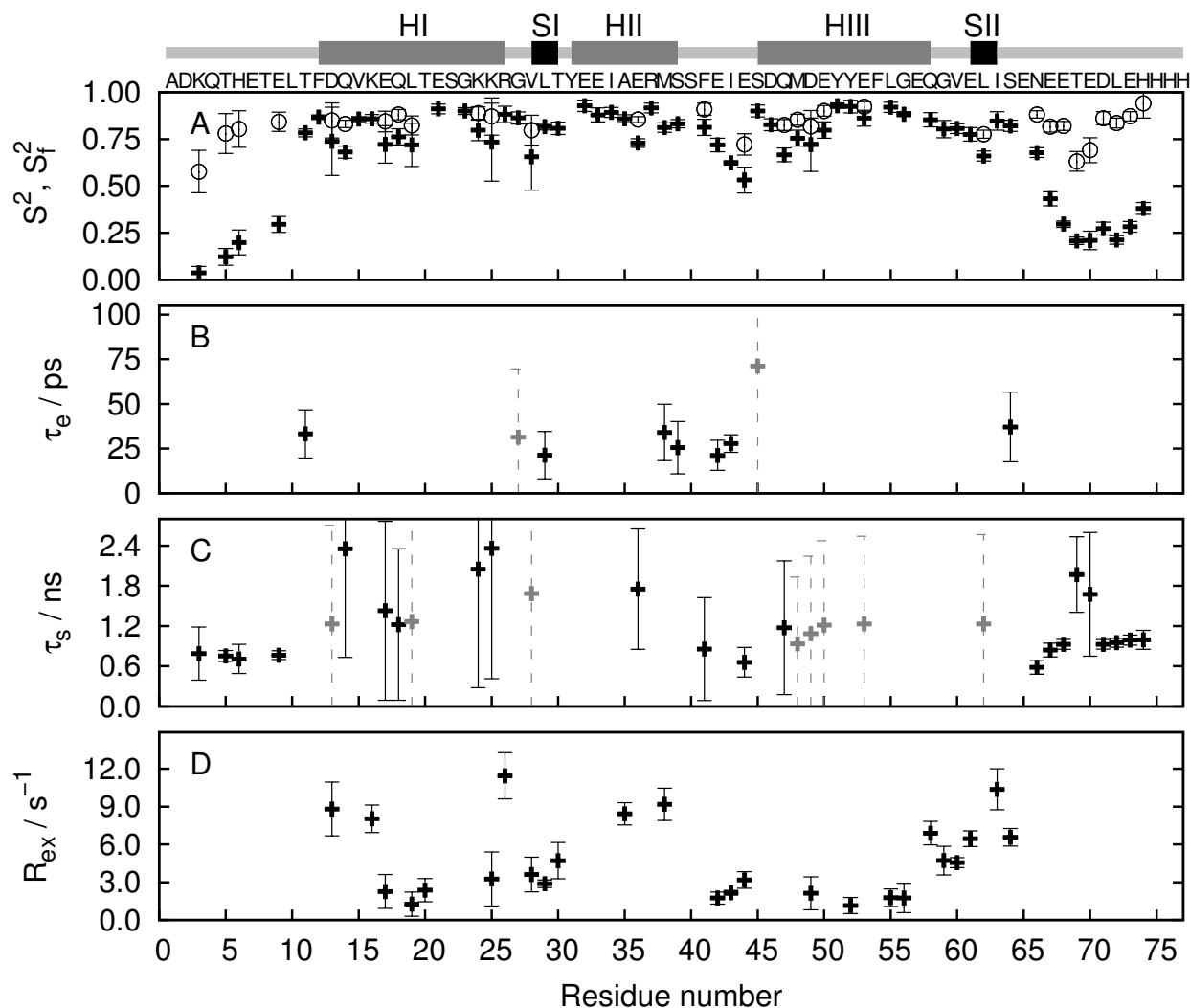


**Figure 2:** Results of model-free analysis of  $R_1$ ,  $R_2$ , and ssNOE measured at 600 MHz, 850 MHz, and 950 MHz spectrometers. (A) Generalised order parameters  $S^2$  (indicated as crosses) and  $S_f^2$  (circles). (B) Effective correlation time  $\tau_e$ . Standard deviations of  $\tau_s$  of S45 was 334 ps. Values of the following residues, exceeding the plotted range, are not shown: E21,  $(1.2 \pm 1.2)$  ns; E33,  $(0.8 \pm 0.7)$  ns; R37,  $(0.7 \pm 0.5)$  ns; and D46,  $(0.9 \pm 0.2)$  ns. (C) Slow timescale correlation time  $\tau_s$ . Standard deviations of  $\tau_s$  of L19 and V28 were 1.6 ns and 1.8 ns, respectively. (D) Exchange contribution  $R_{ex}$ . Fitted correlation times with the standard deviation exceeding 100% are shown in gray. Sequence and secondary structure elements are shown above the graph.

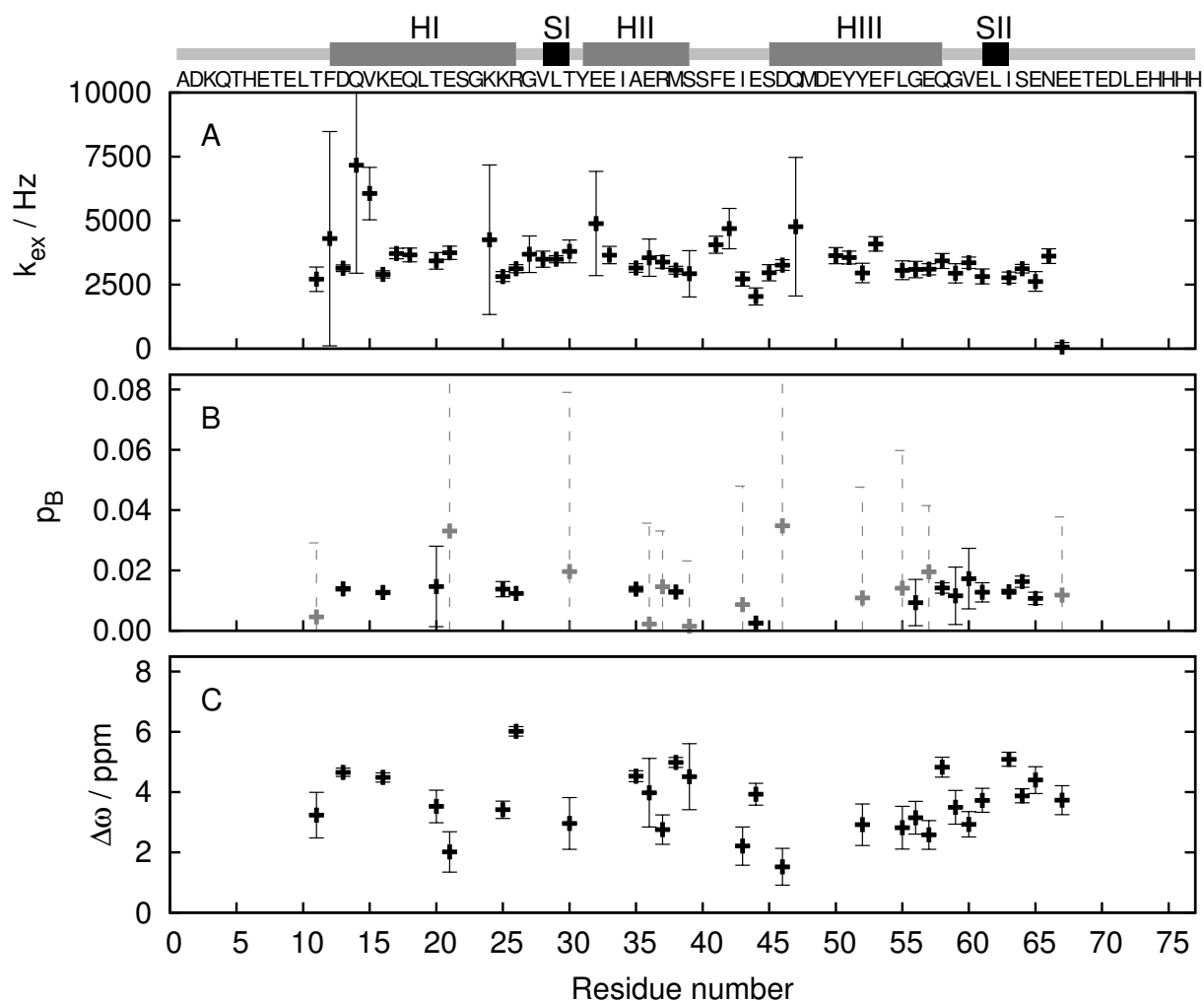


**Figure 3:** Parameters of slow exchange calculated for a two-state model from CPMG relaxation dispersion data obtained at 600 MHz, 850 MHz, and 950 MHz spectrometers. (A) The exchange rate  $k_{\text{ex}}$ . (B) The population of the minor conformational state  $p_B$ . Standard deviations of  $p_B$  of E21 and D46 were 0.087 and 0.089, respectively. (C) The chemical shift difference between the states ( $\Delta\omega$ ). Residues with the standard deviation exceeding 100 % are shown in gray. Sequence and secondary structure elements are shown above the graph.

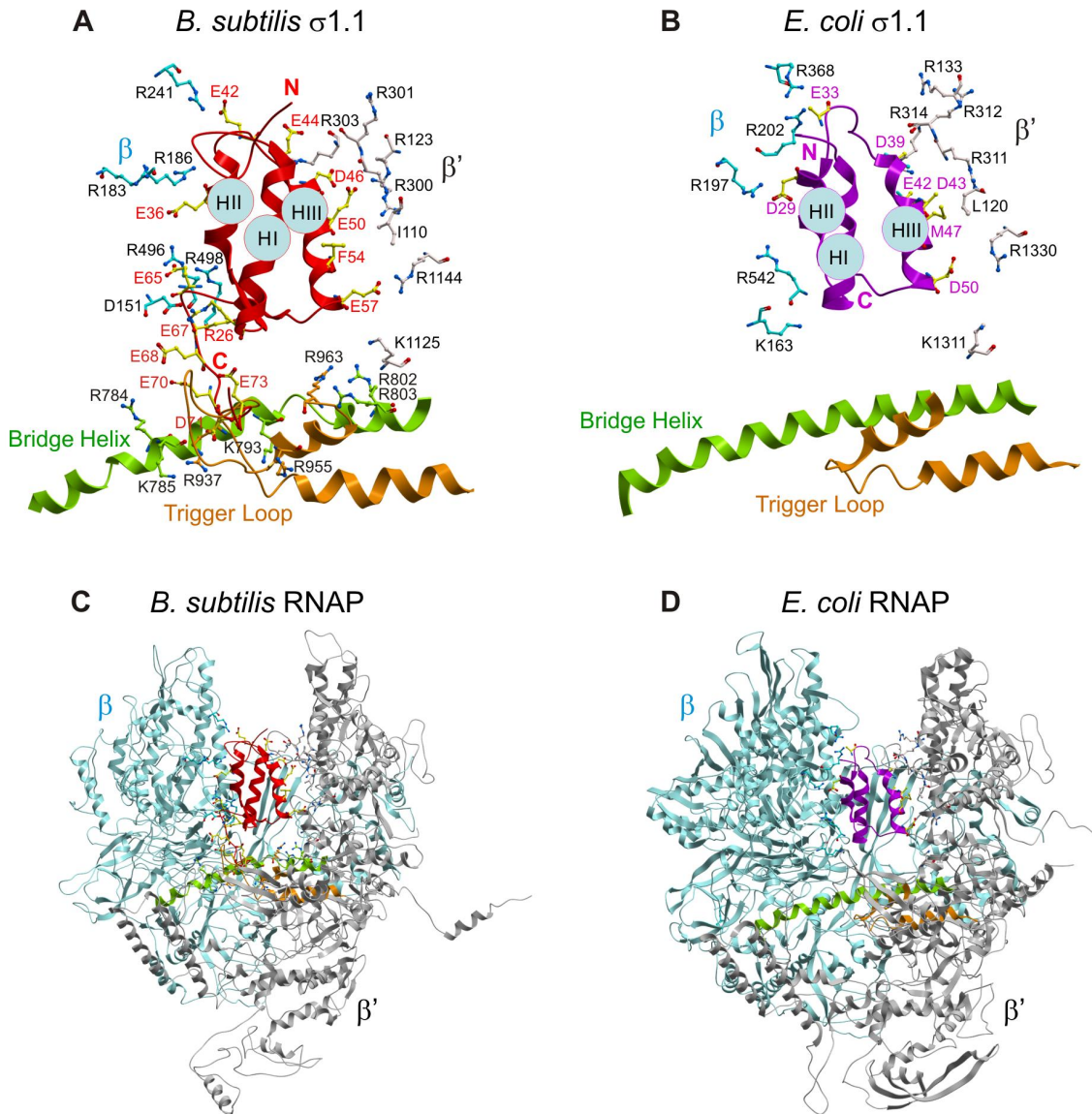


**Figure 4:** Interactions of *B. subtilis* and *E. coli*  $\sigma 1.1$  with RNAP. (A,B) A detail of network of interactions between *B. subtilis* and *E. coli*  $\sigma 1.1$  and  $\beta$ ,  $\beta'$  subunits of RNAP. The  $\sigma 1.1$  domains are shown in red (*B. subtilis*) and magenta (*E. coli*). Side chains of charged amino acids that could form inter-subunit salt bridges are shown in detail. Bridge helix (green) and trigger loop (orange) are indicated. N, C indicate the N- and C-termini of  $\sigma 1.1$ , respectively. (C,D) An overall view of *B. subtilis* (red) and *E. coli* (magenta)  $\sigma 1.1$ . Bridge helix and trigger loop are indicated in the same color coding as in panels A and B.

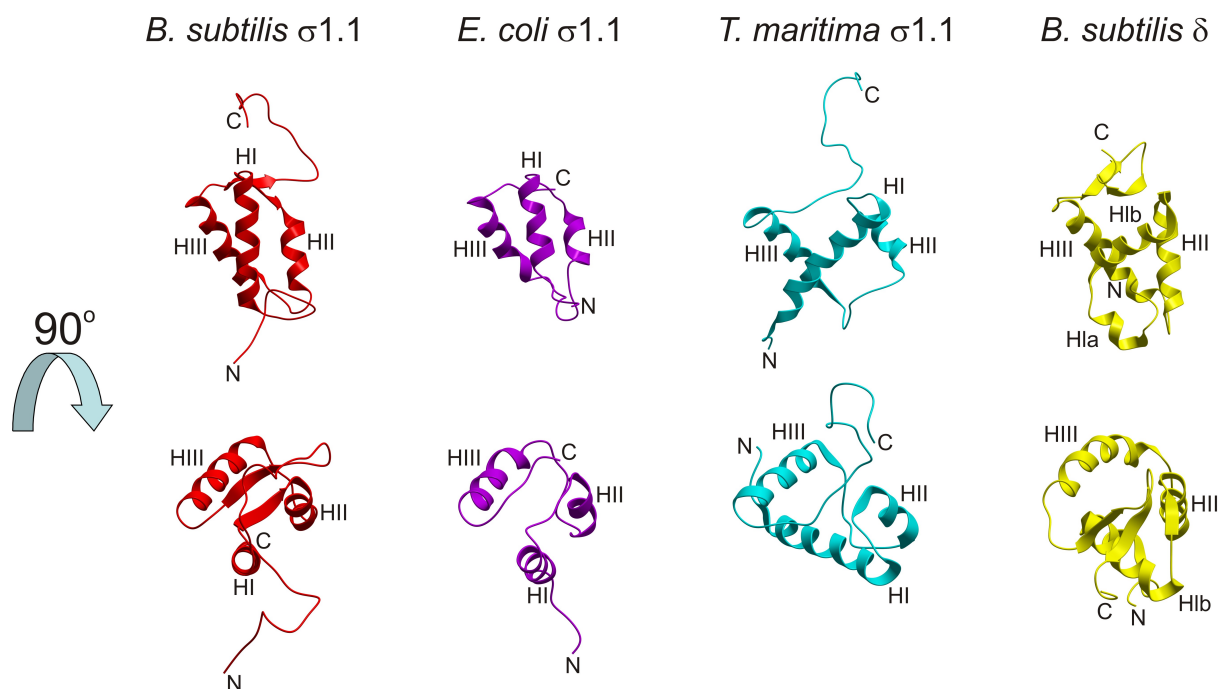


**Figure 5:** Comparison of 3D structures of  $\sigma 1.1$  from *B. subtilis*, *E. coli* and *T. maritima* with the N-terminal domain of the RNAP  $\delta$  subunit from *B. subtilis*.

**Solution Structure of Domain 1.1 of the  $\sigma^A$  Factor from *Bacillus subtilis* is Preformed for Binding to the RNA Polymerase Core**

Milan Zachrdla, Petr Padrta, Alzbeta Rabatinová, Hana Sanderová, Ivan Barvík, Libor Krásný and Lukás Zídek

*J. Biol. Chem.* published online May 24, 2017

---

Access the most updated version of this article at doi: [10.1074/jbc.M117.784074](https://doi.org/10.1074/jbc.M117.784074)

Alerts:

- [When this article is cited](#)
- [When a correction for this article is posted](#)

[Click here](#) to choose from all of JBC's e-mail alerts

Supplemental material:

<http://www.jbc.org/content/suppl/2017/05/24/M117.784074.DC1>

This article cites 0 references, 0 of which can be accessed free at

<http://www.jbc.org/content/early/2017/05/24/jbc.M117.784074.full.html#ref-list-1>